Materials and Structures (2021) 54:115
https://doi.org/10.1617/s11527-021-01707-9

ORIGINAL ARTICLE

Masonry walls retrofitted with natural fibers under tsunami loads

Francesco Fabbrocino · Stefano Belliazzi · Giancarlo Ramaglia · Gian Piero Lignola · Andrea Prota

Received: 11 November 2020 / Accepted: 9 April 2021 / Published online: 10 May 2021

Abstract In the last decades, several tsunamis hit international coasts and engaged scientific awareness to the retrofit of coastal buildings against tsunami loads. Structural design under tsunami loads is difficult due to the high uncertainties of the phenomenon. Local collapse mechanisms of masonry walls, like as out of plane mechanisms, have an high probability due to flexural actions; a higher flexural capacity can be reached using specific retrofit systems; in particular, this paper aims to deepen the behavior of masonry walls retrofitted with innovative retrofit systems like as natural fibers applied with inorganic mortar matrices. The retrofit of structures under tsunami actions could be an innovative research topic for international research community dealing with coastal buildings located in areas characterized by a high tsunami risk. Recent engineering applications demonstrated the innovative strengthening systems to be effective for the retrofit of existing masonry buildings. These strengthening systems are of great interest in the practical applications due to the low costs and their sustainability. In fact, the lower costs compared to the synthetic fibers allow their diffusion in emerging countries. In a first part the impact of constituents on the structural capacity of masonry elements strengthened with natural systems has been discussed. Important results have been provided in order to improve the knowledge and encourage the development of these systems in many engineering applications. Finally, the effects of retrofit systems on masonry walls under tsunami loads will be discussed in terms of critical inundation depth variations before and after the interventions.

Keywords Masonry walls · Local mechanisms · Innovative retrofit systems · Natural fibers · Tsunami

F. Fabbrocino · G. Ramaglia
Department of Engineering, Telematic University Pegaso, Piazza Trieste e Trento, 48, 80132 Naples, Italy

S. Belliazzi · G. P. Lignola (✉) · A. Prota
Department of Structures for Engineering and Architecture, University of Naples Federico II, Via Claudio 21, 80125 Naples, Italy
e-mail: glignola@unina.it

Nomenclature

b_{cs}	Width of the masonry cross-section
$E_{cf,t}$	Young's modulus of fiber
$E_{cm,t}$	Young's modulus of mortar matrix
$E^*_{cm,t}$	Homogenized Young's modulus of composite system
$\overline{E}_{cf,t}$	Dimensionless Young's modulus of fiber
$\overline{E}^*_{cm,t}$	Dimensionless homogenized Young's modulus of composite system
$f_{m,t}$	Tensile strength of masonry
$f_{m,c}$	Compressive strength of masonry
$f_{cm,t}$	Tensile strength of matrix
$f_{cm,c}$	Compressive strength of matrix

$f_{cf,t}$ Ultimate tensile strength of dry fiber
$f^*_{cm,cr}$ Homogenized cracking stress of composite system
$\overline{f}^*_{cm,cr}$ Dimensionless homogenized cracking stress of composite system
g Gravitational acceleration constant
H_i Interstorey height
h Expected inundation depth
h_{cs} Height of the masonry cross-section
h_{max} Design inundation depth
k Constant coefficient
M Bending moment
m Dimensionless bending moment
m_s Dimensionless bending moment
$m_{s,1}$ Dimensionless bending moment equation in case of triangular load pattern
$m_{s,2}$ Dimensionless bending moment equation in case of trapezoidal load pattern
P Axial load
P_m Concentrated load
p Dimensionless axial load
q_{max} Tsunami distributed load at the base of the structure
s Masonry wall thickness
t_{cf} Equivalent thickness of fiber
t_{cm} Thickness of mortar matrix
x Neutral axis depth
α Wall openings ratio
β Fictitious coefficient
$\varepsilon_{cf,t}$ Ultimate strain of composite system
ε_{cm} Generic strain value of composite system
ε_{mu} Ultimate strain of masonry
ε_{m0} Strain value of masonry corresponding to peak value of strength
$\varepsilon_{cm,2}$ Ultimate strain of constant behavior of composite system
$\varepsilon_{cm,cr,1}$ Cracking strain of composite system
$\overline{\varepsilon}$ Dimensionless strain level of composite
λ Factor that correlates the actual distance of the centroid of non-linear stress–strain distribution to the neutral axis depth
η Inundation depth coefficient
ψ Factor that correlates the real nonlinear stress distribution to the stress block resultant
ρ Water density
ρ_c Ratio between area of mortar matrix and of fiber
$\overline{\sigma}^*_c$ Dimensionless stress value of composite
ω_c Mechanical composite reinforcement ratio
ξ Dimensionless neutral axis

1 Introduction

In the last decades several catastrophic tsunami events have stimulated the attention of the scientific community to deepen the behavior of structures under tsunami loads. Post-event surveyors in Sumatra (2004) and Japan (2011) reported a high vulnerability of masonry buildings subjected to tsunami loads compared to other construction types as RC buildings, especially against the activation of out-of-plane mechanisms [1–3].

Clarifying the behavior of masonry walls under tsunami loads in terms of activation of local mechanisms is not obvious because tsunami forces are superficial actions that depend on the exposed surface of the structure to the tsunami waves [4, 5]. Conversely, for instance, seismic forces are inertia actions depending both on the mass and on the dynamic behavior of the structure. Therefore, the behavior of structures under tsunami loads is not comparable to that under seismic loads.

Main flexural out-of-plane local mechanisms are related to vertical [4] and horizontal [6, 7] bending mechanisms; in this paper, only vertical bending mechanisms are analyzed in detail.

In order to increase the existing building capacity against the activation of local mechanisms, the use of composite materials like as natural fibers could be a sustainability criterion.

Composite materials are made of a matrix component (organic or inorganic solution) and a fiber component (synthetic or natural). For masonry materials the organic matrix is generally replaced by the inorganic material [8, 9] due to the best compatibility with the substrate [8, 9]. When the strengthening strategies are performed on high quality masonries, the composite systems based on inorganic matrix and synthetic fibers (i.e. carbon, glass and basalt) are certainly preferable for the strengthening strategy [10]. However, for masonry materials, recent scientific studies [11] have demonstrated that small quantities of composite are enough to adequately improve the structural capacity of the masonry. Furthermore,

masonry elements reinforced with high reinforcement ratios of the composite show a failure mode due to the strengthening system favoring a brittle behavior [12]. The strong differences in terms of mechanical performances between the masonry and the composite promote a low efficiency of the strengthening strategy. Therefore, especially for poorly built masonry buildings, stronger materials might show some drawbacks. In fact, when the strengthening system is applied on poor masonry, the synthetic fibers are generally replaced by natural fibers [13]. The high compatibility in terms of mechanical properties between the composite and the masonry promotes a high efficiency of the strengthening system.

The high mechanical compatibility is not the only advantage of these systems. In particular, intervention strategies performed on heritage buildings must be compatible with the reversibility and restoration criteria [14, 15]. Strengthening systems made of organic matrix and high-performance materials often do not satisfy them. Natural fibers have low cost and are easily available. This is a key aspect to promote the development of strengthening strategies in emerging countries. Furthermore, the strengthening systems based on natural materials satisfy the sustainability criteria due to the manufacturing and life cycle that produce an extremely low pollution. The inorganic matrix can be made of several materials like as cementitious or lime mortar. The choice of the system depends on the characteristics both of the masonry substrate and of the fiber. The mechanical performances of the mortar provide negligible impact in composites based on high performance fiber. This effect is due to the low level of the initial cracking stress compared to the ultimate stress of the composite. In fact, only for inorganic matrices characterized by high mechanical performances, the cracking condition provides a non-null contribution on the structural behavior of the strengthened masonry cross-section.

Furthermore, the ductility is strongly influenced by the cracking threshold [16]. Therefore the structural behavior of the strengthened masonry is strongly influenced by the ratio between the tensile strength of matrix, $f_{\mathrm{cm},t}$ and the tensile strength of the fiber, $f_{\mathrm{cf},t}$. The composite retrofit system guarantees a tensile capacity to the masonry wall cross section and it is a significant improvement for the cross section behavior due to the negligible tensile strength of unreinforced masonry, depending on the layout of fibers [17, 18] and even low amounts of fibers are able to provide significant enhancement, in particular at reduced axial loads [19–21].

Present work focuses on the structural behavior of masonry buildings strengthened with inorganic matrix and natural fiber and subjected to tsunami loads. In a first step, the impact of the inorganic matrix on the ultimate behavior of masonry elements strengthened with natural systems (i.e. inorganic matrix and natural fiber) has been assessed. For these strengthened systems the ultimate condition is generally due to the failure of the composite. Therefore, the value of the cracking threshold modifies the ultimate behavior of the strengthened masonry. The influence of the matrix has been checked in terms of flexural capacity and ductility capacity of the strengthened masonry elements. A parametrical analysis has been carried out considering appropriate values for the stress–strain relationships of masonry and composite system. Successively, the behavior of masonry walls against the activation of bending local mechanisms under tsunami loads is analyzed and the benefits of the retrofit systems with natural fibers are remarked. A useful tool is provided with the aim to design retrofit systems depending on a critical parameter for tsunamis such as the expected inundation depth. The proposed approach and the relative tool are useful for the risk mitigation in areas where masonry buildings show high vulnerability to tsunami loads [22, 23]. All the results are provided in dimensionless form in order to offer generalizable results applicable to any masonry cross section and condition. A practical example has been done according to a linear stress–strain constitutive relationship of composite. This simplified assumption was assumed according to the modern guidelines [24, 25].

2 Retrofit system with natural fibers

A strengthened masonry cross-section is made of several constituents: masonry, mortar matrix and fiber. For each material a specific stress–strain constitutive relationship can be chosen. Many experimental tests showed the masonry to be strongly non-linear already for low stress levels both in compression and in tension [26]. Furthermore, the tensile strength of masonry, $f_{m,t}$ is lower than its compressive strength,

$f_{m,c}$. Usual engineering applications were designed under the no tensile strength assumption for masonry. Recent scientific works [11, 12] showed the impact of this parameter on the ultimate behavior of masonry elements in terms of flexural and ductility capacities [13]. For strengthened elements, the tensile strength of masonry provides negligible impact on the flexural capacity. However, the influence on the ductility could be not negligible [12].

The goal of this first part is to assess the impact of the mechanical properties of matrix on the ultimate behavior of the strengthened masonry. Therefore, the influence of the tensile strength of masonry on the structural behavior of the strengthened masonry has been neglected.

2.1 Mechanical and geometrical characterization

The masonry has been modelled in compression by means of the simplified stress–strain constitutive relationship according to Eurocode 6 [27]. It is represented by two main stress–strain relationships: a first parabolic stress–strain relationship starting from the origin up to a conventional strain value equal to $\varepsilon_{m0} = 0.002$; a second constant stress–strain relationship starting from the ε_{m0} up to the conventional ultimate strain, $\varepsilon_{mu} = 0.0035$ with a maximum stress equal to the compressive strength of masonry, $f_{m,c}$ (Fig. 1).

Recent experimental tests provided important information on the structural behavior of composites [28]. The recent scientific studies [29, 30] show that the stress–strain constitutive relationship is strongly influenced by the constituents (i.e. matrix and fiber).

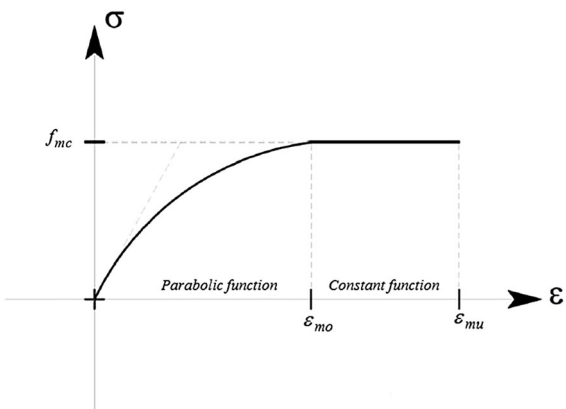

Fig. 1 Stress–strain constitutive relationships for masonry

For strengthening systems made of inorganic matrices and natural fibers, experimental results show three main behavior thresholds on the stress–strain constitutive relationship. Therefore, the composite can be modelled by using a tri-linear simplified stress–strain relationship. The strengthening system has been considered effective only under tensile stress. Mortar matrix and fiber differ both in terms of tensile strength ($f_{\mathrm{cm},t}$ and $f_{\mathrm{cf},t}$) and of elastic properties. The mortar matrix has thickness, t_{cm} and Young's modulus, $E_{\mathrm{cm},t}$; conversely, the fiber has equivalent thickness, t_{cf} and Young's modulus, $E_{\mathrm{cf},t}$. The stress–strain constitutive relationship can be easily homogenized considering a composite system with thickness of the fibers. The initial stress–strain constitutive relationship has an homogenized Young's modulus, $E^*_{\mathrm{cm},t}$:

$$E^*_{\mathrm{cm},t} = \frac{E_{\mathrm{cm},t} \cdot t_{\mathrm{cm}} + E_{\mathrm{cf},t} \cdot t_{\mathrm{cf}}}{t_{\mathrm{cf}}} \tag{1}$$

The previous equation provides the initial stress–strain constitutive relationship up to the homogenized cracking stress, $f^*_{\mathrm{cm,cr}}$ (green line of Fig. 2):

$$\begin{aligned} f^*_{\mathrm{cm,cr}} &= \frac{f_{\mathrm{cm},t}}{E_{\mathrm{cm},t}} E^*_{\mathrm{cm},t} = \frac{f_{\mathrm{cm},t}}{E_{\mathrm{cm},t}} \left(E_{\mathrm{cm},t} \frac{t_{\mathrm{cm}}}{t_{\mathrm{cf}}} + E_{\mathrm{cf},t} \right) \\ &= f_{\mathrm{cm},t} \left(\frac{t_{\mathrm{cm}}}{t_{\mathrm{cf}}} + \frac{E_{\mathrm{cf},t}}{E_{\mathrm{cm},t}} \right) \end{aligned} \tag{2}$$

For a value of the strain, $\varepsilon_{\mathrm{cm}}$ higher than the cracking strain (blue line of Fig. 2), $\varepsilon_{\mathrm{cm,cr},1}$:

$$\varepsilon_{\mathrm{cm,cr},1} = \frac{f_{\mathrm{cm},t}}{E_{\mathrm{cm},t}} = \frac{f^*_{\mathrm{cm,cr}}}{E^*_{\mathrm{cm},t}} \tag{3}$$

the homogenized cracking stress, $f^*_{\mathrm{cm,cr}}$ remains constant up to the strain $\varepsilon_{\mathrm{cm},2}$:

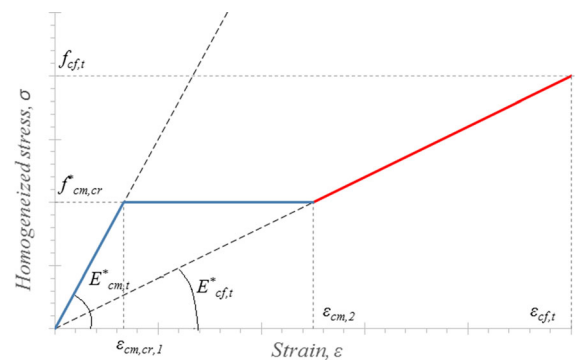

Fig. 2 Stress–strain constitutive relationships for and the composite system

$$\varepsilon_{cm,2} = \frac{f^*_{cm,cr}}{E_{cf,t}} \tag{4}$$

For a strain value higher than, $\varepsilon_{cm,2}$ the behavior of the composite is governed by the fiber (red line of Fig. 2). Therefore, the ultimate condition of the composite is due to the failure of the fiber, i.e. point ($f_{cf,t}$, $\varepsilon_{cf,t}$) of Fig. 2.

In this paper, the influence of the cracking threshold, $f^*_{cm,cr}$, on the ultimate behavior of strengthened masonry has been assessed.

2.2 Dimensionless approach

The flexural capacity of a strengthened masonry can be written dimensionless according to the method explained in [13]. The flexural capacity has been derived starting from the bending moment–curvature diagram, M-χ. Once the axial load is fixed, the points along the vertical line on the P-M domain represent different behaviors at increasing curvature in the plane M-χ up to the flexural capacity. The normalization allows to provide generalizable results for any geometric and mechanical parameters. For a generic cross-section, the dimensionless parameters, p and m, axial load and bending moment, respectively, can be introduced:

$$p = \frac{P}{b_{cs} \cdot h_{cs} \cdot f_{m,c}} \tag{5}$$

$$m = \frac{M}{b_{cs} \cdot h_{cs}^2 \cdot f_{m,c}} \tag{6}$$

where b_{cs} and h_{cs} represent the width and height of the masonry cross-section respectively, $f_{m,c}$ is the compressive strength of the masonry, P and M are the axial load and bending moment, respectively.

The normalization has been performed with reference to the ultimate tensile strength of the dry fiber, $f_{cf,t}$. For the trilinear stress–strain constitutive relationship of the composite the homogenized moduli, $E^*_{cm,t}$ and $E_{cf,t}$ and cracking stress, $f^*_{cm,cr}$, can be normalized as follow:

$$\overline{E}^*_{cm,t} = \frac{E^*_{cm,t}}{f_{cf,t}} \tag{7}$$

$$\overline{E}_{cf,t} = \frac{E_{cf,t}}{f_{cf,t}} \tag{8}$$

$$\overline{f}^*_{cm,cr} = \frac{f^*_{cm,cr}}{f_{cf,t}} \tag{9}$$

It is interesting to note that $\overline{E}^*_{cm,t}$ and $\overline{E}_{cf,t}$ represent the reciprocal of a strain.

In addition, each representative strain of the composite stress–strain constitutive model is dimensionless depending on the ultimate strain $\varepsilon_{cf,t}$.

Assuming perfect bond between masonry and composite, the stress–strain constitutive relationship can be expressed in normalized form as follow:

$$\overline{\sigma}^*_c = \begin{cases} \overline{\varepsilon} \cdot \overline{E}^*_{cm,t} \rightarrow -\overline{\varepsilon}_{cm,cr,1} \leq \overline{\varepsilon} \leq 0 \\ \overline{f}^*_{cm,cr} = \overline{E}^*_{cm,t} \cdot \overline{\varepsilon}_{cm,cr,1} \rightarrow -\overline{\varepsilon}_{cm,2} < \overline{\varepsilon} < -\overline{\varepsilon}_{cm,cr,1} \\ \overline{\varepsilon} \cdot \overline{E}_{cf,t} \rightarrow -\overline{\varepsilon}_{cf,t} \end{cases} \tag{10}$$

where, $\overline{\varepsilon}$ is the dimensionless strain level of the composite (i.e. equal to the strain value of the masonry substrate in perfect bond) and, $\overline{\sigma}^*_c$ is the dimensionless stress value achieved by the composite. For a reinforced masonry cross section, with unitary depth, the ratio between the mortar matrix and the fiber, ρ_c, is introduced:

$$\rho_c = \frac{t_{cm}}{t_{cf}} \tag{11}$$

The stress–strain constitutive relationship can be expressed by means of normalized parameters: $\overline{E}^*_{cm,t}$, $\overline{E}_{cf,t}$, $\overline{f}^*_{cm,cr}$ and ρ_c.

The neutral axis, x, can be normalized with respect to cross section height, $\xi = x/h$. The equilibrium equations on the reinforced concrete cross-section can be written introducing the mechanical reinforcement ratio, ω_c as follows:

$$\omega_c = \frac{t_{cf} \cdot f_{cf,t}}{h_{cs} \cdot f_{m,c}} \tag{12}$$

Therefore, the horizontal equilibrium equation can be written in normalized form:

$$p = \psi \cdot \xi + \omega_c \cdot \bar{\sigma}_c \tag{13}$$

where: ψ is the factor that correlates the real nonlinear stress distribution to the stress block resultant; it is a function of the maximum masonry strain [31]. The

flexural capacity can be evaluated according to rotational equilibrium around the centroid of the cross section as follows:

$$6 \cdot m = -(1-\lambda) \cdot \psi \cdot \xi^2 + \psi \cdot \xi - 0.5 \cdot p \qquad (14)$$

where, λ is the factor that correlates the actual distance of the centroid of non-linear stress–strain distribution to the neutral axis depth, x (Fig. 3). It is function of the maximum masonry strain. In the previous equations, p and m are functions only of the previously discussed normalized parameters.

2.3 Parametrical analysis

Parametrical analysis has been carried out fixing appropriate values for the normalized stress–strain relationships of masonry and composite systems. The following analysis was performed according to a research-oriented approach. In fact, the available models [24, 25] neglect the influence of the mortar matrix on the structural capacity of the strengthened masonry. The goal of this analysis is to provide the key effect of constituents on the structural behavior of strengthened masonry cross-sections. The numerical results are dimensionless [13]. The main objective is to analyze the mechanical performance of the reinforced masonry at the variation of the mortar matrix. The choice of the mechanical and geometrical parameters for the parametrical analysis was carried out by analyzing the natural fibers and mortar matrices commercially available. The properties for the dry natural fibers were defined according to average properties. This allowed to fix a specific range of the mechanical properties for mortar matrix. Table 1 outlines the values of the geometrical and mechanical parameters chosen for the composite systems.

The cracking stress, $\overline{f}^{*}_{cm,cr}$ has been changed up to the limit condition where the homogenized cracking stress, $\overline{f}^{*}_{cm,cr}$ is equal to the tensile strength of the dry natural fiber, $\overline{f}_{cf,t}$. Starting from the values reported in Table 1, the normalized parameters have been estimated according to the previously discussed approach (Table 2).

Therefore, the parametrical analysis was carried out with five normalized models of the natural composites, by changing only the properties of the mortar (Fig. 4).

The mechanical fiber reinforcement ratio, ω_c varies from 0 to 2 by using the following steps: 0, 0.1, 0.25, 0.5, 1 and 2. The following figures show the bending moment–curvature diagrams for the five stress–strain models while changing the reinforcement ratio, ω_c. For this analysis the axial load, P is assumed equal to 20% of the axial strength. Figure 5 shows the comparison between the model 1 ($\overline{f}^{*}_{cm,cr} = 0$) and the model 2 ($\overline{f}^{*}_{cm,cr} = 0.1$). The black dashed line reported in the following figures represents the bending moment–curvature diagram of the unreinforced masonry element (i.e. $\omega_c = 0$).

When the tensile strength of the matrix is reduced, the trilinear relationship (model 2) tends to provide results that are similar to the linear relationship of the fiber alone (model 1). The negligible influence is clear also for different values of the reinforcement ratios, ω_c. For these systems also the influence of the tensile strength of matrix on the ductility capacity results negligible. Figure 6 shows the comparison between the model 1 ($\overline{f}^{*}_{cm,cr} = 0$) and the model 3 ($\overline{f}^{*}_{cm,cr} = 0.33$).

The influence of the tensile strength of the matrix is clear for different mechanical fiber reinforcement ratios. The ultimate curvature (evaluated at a drop of 20% after peak bending moment) decreases with the tensile strength of the matrix. Therefore, this

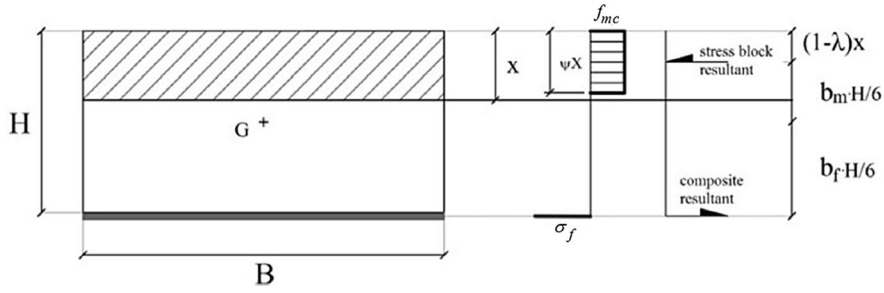

Fig. 3 Strengthened masonry cross-section: internal stresses and dimensionless parameters

Table 1 Geometrical and mechanical properties of the natural composite

Element	Tensile strength (MPa)	Young's modulus (GPa)	Thickness (mm)
Hemp grid	47	7	0.3
Mortar	0, 0.1, 0.35, 0.75, 1.05	8	15

Table 2 Normalized parameters for the natural composite

Model	$\overline{E}^{*}_{cm,t}$ [–]	$\overline{E}_{cf,t}$[–]	$\overline{f}^{*}_{cm,cr}$ [–]	$\overline{\varepsilon}_{cm,cr,1}$ [–]	$\overline{\varepsilon}_{cm,2}$ [–]
Model 1	7617	149	0	0.000	0.000
Model 2			0.1	0.002	0.095
Model 3			0.33	0.007	0.333
Model 4			0.71	0.014	0.714
Model 5			1	0.020	1.000

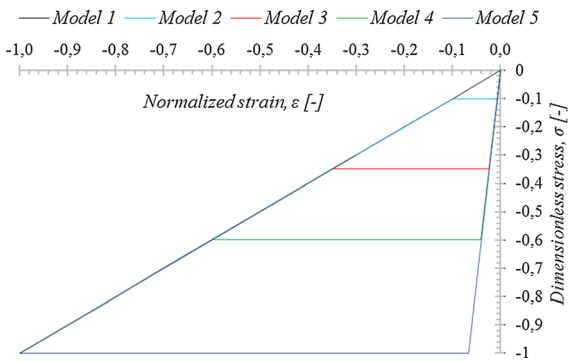

Fig. 4 Normalized stress–strain constitutive relationships for the composite: model 1 (black line), model 2 (pale blue line), model 3 (red line), model 4 (green line) and model 5 (dark blue line). (Color figure online)

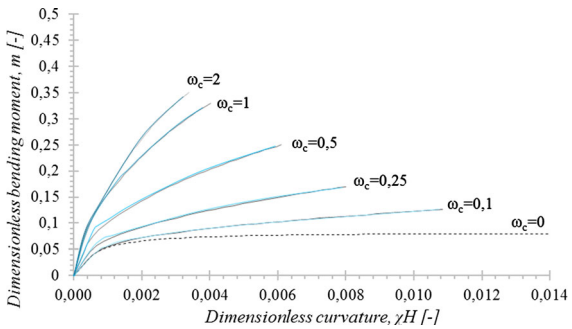

Fig. 5 Normalized bending moment–curvature diagrams: model 1 (black lines), model 2 (pale blue lines). (Color figure online)

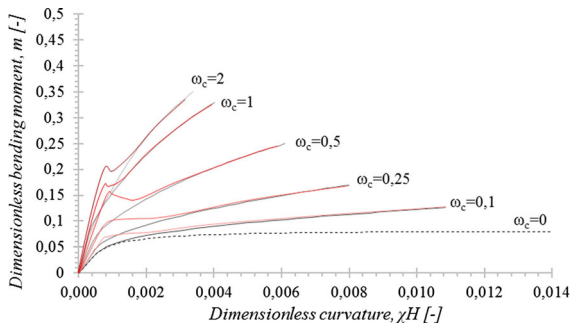

Fig. 6 Normalized bending moment–curvature diagrams: model 1 (black lines), model 3 (red lines). (Color figure online)

parameter influences the ductility capacity of the strengthened masonry cross-section. For higher reinforcement ratios the impact of the mortar becomes negligible also for the model 3. In fact, for high reinforcement ratios the failure mode is constantly due to the masonry and the tensile strength of matrix changes the bending-moment diagram only for low fiber strength levels. Figure 7 shows the comparison between the model 1 ($\overline{f}^{*}_{cm,cr} = 0$) and the model 4 ($\overline{f}^{*}_{cm,cr} = 0.71$).

Similar results can be observed for the model 4. When the tensile strength increases, the effect of the cracking stress is not negligible. For high performance mortar matrix, the ultimate condition of the masonry

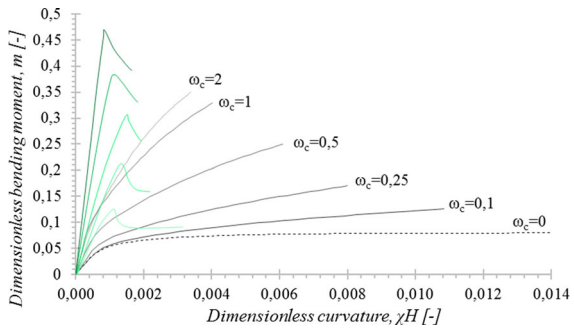

Fig. 7 Normalized bending moment–curvature diagrams: model 1 (black lines), model 4 (green lines). (Color figure online)

cross-section is due to the failure of matrix. This effect has been remarked in Fig. 8 by means of the comparison between the model 1 and model 5 (i.e. homogenized tensile strength of mortar equal to the tensile strength of fiber). In this case the flexural behavior of the strengthened masonry cross-section is weakly influenced by the reinforcement ratio and the failure mode is brittle.

3 External loads

The modelling of the wave impact on the structures is difficult due to the different components of the tsunami. In particular, hydrostatic loads, hydrodynamic loads and debris impact forces characterize the main horizontal loads. In the scientific literature different codes and guidelines provide different approaches for modelling tsunami forces on structures; the main international references are provided by ASCE 7–16 [32], FEMA P-646 [33] and Japanese guideline [34].

Two different approaches can be recognized in the cited documents: the first one is developed and proposed by FEMA and ASCE that consider several scenarios and forces (e.g., hydrostatic, drag, buoyant, surge, impact, debris impact forces). Every force depends on several parameters (e.g., inundation depth, flow velocity and maximum momentum flux) indicated by hazard maps, numerical simulations or simplified equations.

The second approach is defined by the Japanese guideline and it is based on the assumption that the tsunami loads on buildings can be modelled adopting one equivalent hydrostatic load that implicitly

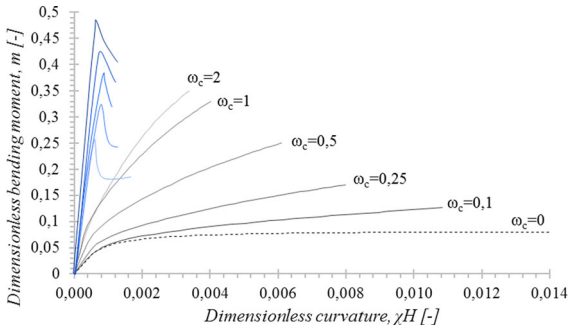

Fig. 8 Normalized bending moment–curvature diagrams: model 1 (black lines), model 5 (dark blue lines). (Color figure online)

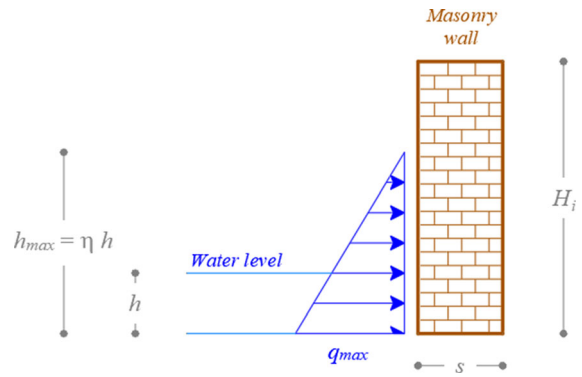

Fig. 9 Equivalent hydrostatic load on a masonry wall characterized by an interstorey height H_i and thickness s

includes hydrostatic and hydrodynamic loads (Fig. 9). In particular, the fictitious design inundation depth $h_{\max}$ is assumed equal to the expected inundation depth h amplified by a coefficient η depending on availability of specific tsunami energy dissipation structures, namely seawalls; the coefficient η is variable between 1.5 and 3.0 and the expected inundation depth is the only parameter needed to model tsunami loads on structures, including implicitly also dynamical effects of the tsunami wave upon the impacted structure. Therefore, the distributed load $q_{\max}$ at the base of the structure is evaluated according to the following equation:

$$q_{\max} = \rho g(\eta \boldsymbol{h}) \tag{15}$$

where ρ is the water density and g the gravitational acceleration constant.

The Japanese guidelines follow the basic concept proposed in the previous guideline by [35] where the coefficient η is always equal to its maximum value. The method has been revisited because the coefficient η was too conservative considering tsunami post-event measurements.

Therefore, the Japanese approach is adopted to carry out analyses on coastal masonry buildings considering η equal to its maximum value, due to the absence of any tsunami energy dissipation structures.

4 Vertical bending mechanism

In this paper, the activation of out-of-plane local mechanisms is investigated mainly as vertical bending

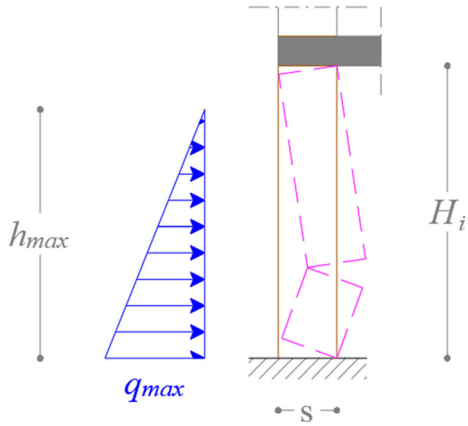

Fig. 10 Vertical bending mechanism

mechanism for a masonry wall under tsunami loads [22] (Fig. 10).

As shown in Fig. 10, the section that reaches the failure and yields to the collapse of the wall is at the lower part of the wall due to the considered external load pattern. In fact, it is interesting to note that seismic forces are inertia forces depending on the mass of the structure while tsunami actions are superficial forces that depend on the exposed surface of the structure to the tsunami waves.

In the next paragraph normalized *P-M* interaction diagrams of the wall cross section and normalized maximum external bending moment equations have been developed in order to evaluate the critical inundation depth that activates the vertical bending mechanism of masonry walls under tsunami loads. In addition, the bending capacity of the wall cross section is increased by the retrofit system with natural fibers to account for the effect of retrofitting.

4.1 P-M interaction diagrams

As shown in Sect. 2.1, the behavior of composite systems, generally, is variable due to the interaction between the matrix and the fibers. In fact, composites have a linear behavior before matrix cracking and subsequent tension stiffening at low strain values.

In the masonry wall analysis, a linear behavior is assumed to describe the composite retrofit system (i.e. Model 1) while capacity in compression is neglected as basic assumption, coherently with a design-oriented approach. In fact, a linear behavior is assumed to describe the composite stress–strain relationship due to the assumption of cracked mortar according to main international guidelines as CNR DT 215 [25] and ACI 549.4R-13 [24]. Therefore, in Eq. 10, the cracking stress $f_{\mathrm{cm,cr}}$ is assumed equal to zero while the elastic modulus $E_{\mathrm{cm},t}$ becomes irrelevant.

The masonry behavior in compression is described according to the Eurocode 6 [27], see Sect. 2.1.

Furthermore, on the top, an additional concentrated load P_m is to be considered for modelling self-weight and the effect of other storeys. Therefore, a normalized external axial load on the cross section is assumed variable in a range up to about 40% of the ultimate axial load capacity of the walls. The corresponding ultimate bending moment is evaluated based on *P-M* interaction diagrams as P_m value changes.

4.2 Maximum external bending moment

The activation of vertical bending out-of-plane mechanism occurs when maximum external bending moment equals the cross-section capacity.

Linear analyses are performed considering a mechanical model composed by a simply supported beam with a linear (triangular o trapezoidal) load pattern characterized by a variable inundation depth and a constant slope (equal to the water density) according to the Japanese approach where tsunami loads on structures are described adopting one equivalent hydrostatic load. The simply supported beam length is equal to the interstorey height H_i.

Considering the static model shown in Fig. 11, it is easy to derive the maximum of the bending moment function, by considering the zero of the shear function.

Dimensionless equations have been evaluated in the case of triangular ($m_{s,1}$) and trapezoidal ($m_{s,2}$) load patterns in order to compare the external bending moment with the ultimate bending moment of the cross section and to provide generalizable results that can be used for any masonry wall.

$$m_{s,1} = k\eta^3 \left(\frac{h}{s}\right)^3 \frac{s}{H_i} \times \left(9 - 9\eta \frac{h}{s}\frac{s}{H_i} + 2\sqrt{3\eta^3}\left(\frac{h}{s}\right)^{\frac{3}{2}}\left(\frac{s}{H_i}\right)^{\frac{3}{2}}\right) \quad (16)$$

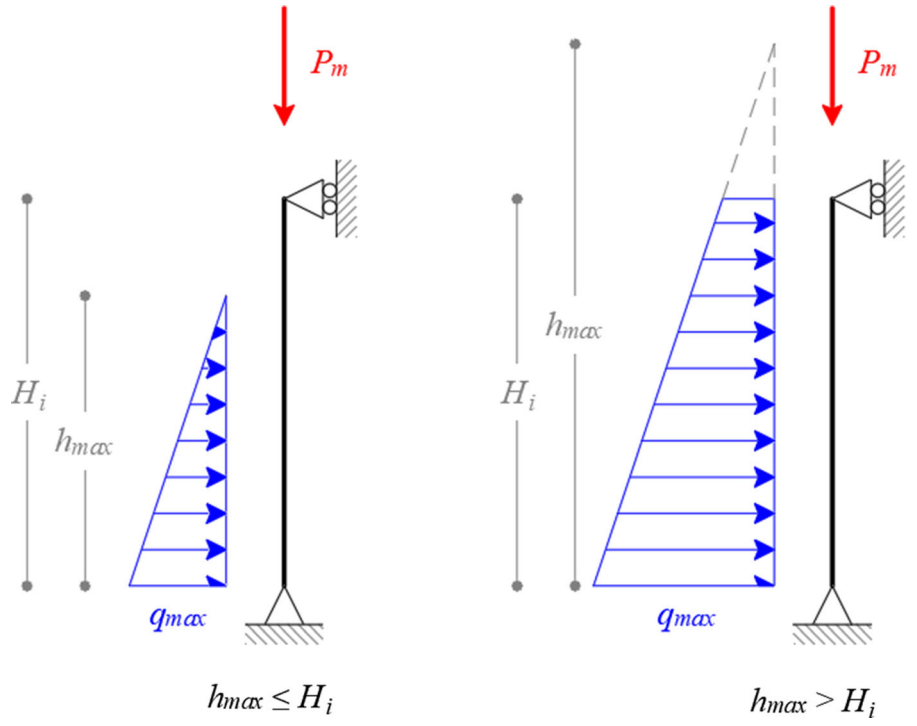

Fig. 11 Static model analyzed with triangular and trapezoidal load patterns

$$m_{s,1} = k\eta^3 \left(\frac{h}{s}\right)^3 \frac{s}{H_i} \times \left(9 - 9\eta \frac{h}{s}\frac{s}{H_i} + 2\sqrt{3\eta^3}\left(\frac{h}{s}\right)^{\frac{3}{2}}\left(\frac{s}{H_i}\right)^{\frac{3}{2}}\right) \quad (17)$$

where:

- $k = \frac{\gamma g \rho H_i}{54 f_{m,c}}$;
- $\beta = \sqrt{3}\sqrt{\left(\frac{H_i}{s}\right)^2 - 3\eta\frac{H_i}{s}\frac{h}{s} + 3\eta^2\left(\frac{h}{s}\right)^2}$;
- α is the wall openings ratio;

The ratio between areas of openings (windows and doors) and of gross wall, (1-α) was assumed to be between 0 and 0.3 according to ASCE 7-16 [32] and the Japanese guidelines [34].

In addition, the equations depend on the ratio s/H_i that represents the geometrical vertical slenderness of the masonry wall.

The previous equations have been plotted for different constant values of the geometrical slenderness of the wall s/H_i considering the ratio m_s/k on the y-axis and h/s on the x-axis (Fig. 12).

The circular marks represent the critical points where the triangular load pattern is substituted by the trapezoidal load pattern; these points are evaluated by the simple equality:

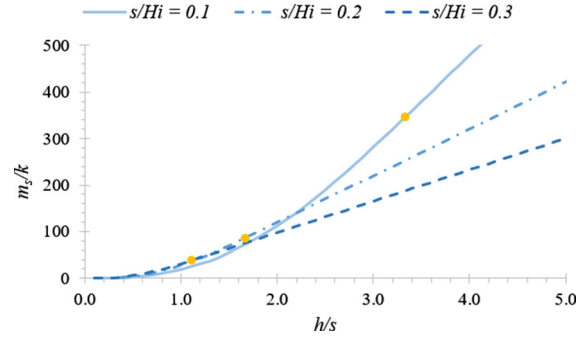

Fig. 12 Normalized critical bending moment

$$\eta h = H_i \rightarrow \frac{h}{s} = \frac{1}{\eta \frac{s}{H_i}} \quad (18)$$

The order of magnitude on y-axis is large due to the dimensionless constant k value that is usually variable in the range 10^{-4} to 10^{-5} and in particular, it depends primarily on the ratio $H_i/f_{m,c}$ because the other parameters can be considered constant in this study.

In addition, in Fig. 12, the curves overlap due to the influence of wall thickness s, despite the external bending moment is independent from the wall thickness. The selection of normalized constant, howsoever, is useful to compare the external bending moment and the bending capacity of the wall cross section.

5 Retrofit system effects

In order to clarify retrofit system effects, several normalized *P-M* interaction diagrams are plotted considering different values of the composite mechanical ratio ω_c, ultimate composite strain ε_u (i.e. $\overline{E}_{\mathrm{cf},t}$ representing the reciprocal of ultimate composite strain) and external normalized axial load values p (Fig. 13). Generally, normalized axial loads in real structures range between 0.1 and 0.4.

For ω_c equal to zero, it is possible to extrapolate the bending capacity of the cross section without retrofit systems (i.e. unreinforced). In addition, it is clear that small increments of composite mechanical ratio provide significant benefits in terms of bending capacity for the cross section. In fact, it is assumed that masonry does not carry tractions and the cross section has no bending capacity at zero axial load while adding a retrofit system to the cross section, that carries only tractions, the benefits at small external axial loads are significant in terms of bending capacity.

It is interesting to note that for high external axial loads, the benefits of a retrofit system are limited by increasing the composite mechanical ratio. This is due to the higher values of neutral axis depth that cause a limited strain in the fibers in tension and, consequentially, a limited fiber contribution.

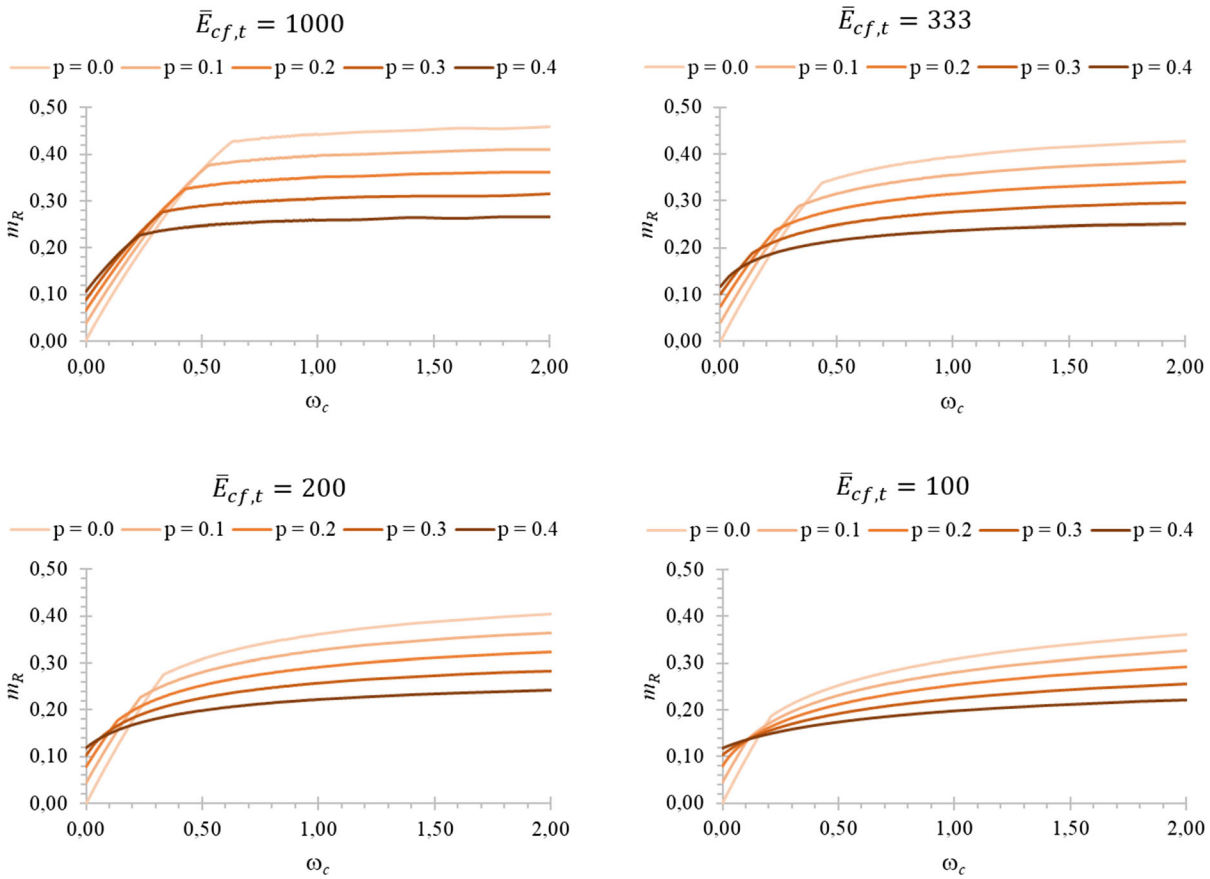

Fig. 13 Ultimate bending moment diagrams of masonry cross section for different composite proprieties and fixed external axial loads, p

The proposed diagrams in Figs. 12 and 13 can be useful to design a retrofit system for existing masonry buildings in tsunami prone areas. A numerical example is reported in order to check the potential of the proposed diagrams. In particular, the minimum composite mechanical ratio to guarantee the minimum structural capacity against the activation of vertical bending mechanisms can be easily evaluated by coupling the proposed diagrams, once the expected inundation depth is given.

For example, it is possible to consider a category of walls having an interstorey height H_i of 4.0 m (Fig. 10), an average compressive strength $f_{m,c}$ of 6.0 MPa and a normalized external axial load p equal to 0.1. For the composite made of natural fibers, an ultimate strain is assumed equal to 5‰ ($\overline{E}_{cf,t} = 200$). In addition, the following assumptions are made for the constant parameters:

- $\alpha = 0.7$;
- $\eta = 3$;
- $g = 9.81$ m/s^2;
- $\rho = 1.1$ ton/m^3.

The density of water ρ assumes that the tsunami flows consist of a mixture of sediment and seawater as reported in FEMA P-646 [33].

In this case, the k parameter is equal to 9.32 10^{-5} and multiplying the external bending moment by k, it is possible to compare the external demand with the capacity of cross section in terms of bending moment (Fig. 14). The ordinate of the chart in Fig. 14 represents the external bending moment for the left side of the chart (as in Fig. 12) and the ultimate bending moment of the retrofitted cross-section for the right

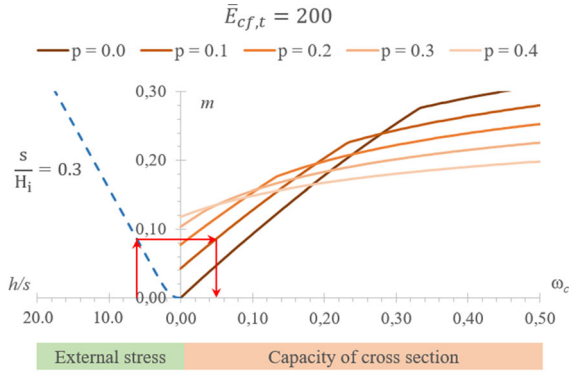

Fig. 14 Comparison between normalized external bending moment (demand) and bending capacity of cross section

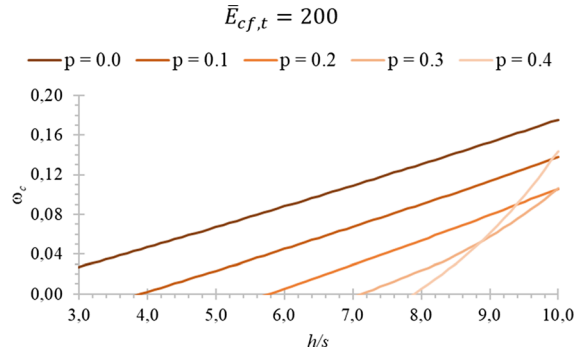

Fig. 15 Design chart of minimum composite mechanical percentage ω_c

side of the chart (as in Fig. 13). The chart assumes the equivalence between the external bending moment and ultimate bending moment of the retrofitted cross-section to estimate the required minimum composite mechanical percentage ω_c. In particular, the input parameter is the dimensionless expected inundation depth h/s. The blue dotted line allows to evaluate the dimensionless external bending moment on the wall related to the external inundation depth h.

A design chart (Fig. 15) can be easily obtained by imposing the equality between the external bending moment (demand) and the ultimate bending moment (capacity) of the wall cross section.

Assuming the ratio between the expected inundation depth h and the wall thickness s equal to 6.0, for the considered wall properties ($p = 0.1$), a minimum composite mechanical ratio of about 4.8% is required. It is evident that at higher axial loads, the increases of composite mechanical ratio become less significant, as the failure is mainly due to masonry.

6 Concluding remarks

This paper aimed to clarify the effects of retrofit systems with natural fibers against the activation of vertical bending mechanisms in a masonry wall under tsunami loads. In addition, the behavior of masonry sections strengthened with natural composite systems was evaluated when varying the different mechanical parameters. The variability of the behavior has been analyzed, changing both the reinforcement ratios and the mechanical properties of the matrix. All results were provided by using a dimensionless process.

In practical applications, prescriptive approaches are generally used to design the reinforcement systems. They generally lead to an overestimation of the effective amount of required reinforcement. The first analysis contributes to the implementation of performance-based design. The type of reinforcement can be selected in order to optimize the structural behavior of the strengthened masonry. For natural systems, the structural behavior of the strengthened masonry becomes strongly dependent on the mechanical properties of the matrix. Natural systems characterized by high performance matrices and excessive reinforcement ratios provide deleterious effects in terms of ductility and efficiency of the intervention strategy, in fact the failure becomes totally brittle. This represents a key aspect in the assessment and strengthening, especially for poor masonry. For these masonries, the use of compatible materials, like as natural fibers and limited strength mortar matrices, appears to be the best solution to improve the structural capacity. However, the choice of the constituents is important in order to optimize the structural behavior. Previous analyses have shown the deleterious effects of high-performance matrices coupled with natural fibers and deleterious effects of excessive reinforcement ratios on ductility. These first results become critical for composites where the constituents present similar performances. It is generally achievable for systems made of natural fibers. In fact, when the natural fiber is replaced by synthetic materials the impact of the performance of the mortar matrix could be negligible.

Composite retrofit systems with natural fibers are one of the most useful techniques for retrofitting existing buildings due to high durability and fire resistance of materials and sustainability criteria. In fact, these strengthening systems are generally characterized by small thickness compared to the wall thickness. Therefore, they do not influence the dynamic characteristics of the structure due to the negligible mass. In addition, the fiber mesh guarantees an improvement of bending moment strength of the retrofitted element.

When the ratio between the tensile strength of fiber and the tensile strength of mortar matrix increases, the linear stress–strain constitutive relationship appears to be the best strategy to model the composite. Linear analyses were performed considering a mechanical model composed by a simply supported beam with a linear (triangular o trapezoidal) load pattern characterized by a variable inundation depth as reported in the Japanese guideline that considers one equivalent hydrostatic load to fully describe the tsunami loads.

Furthermore, a linear behavior is assumed to describe the mechanical behavior of composite strengthening system with natural fibers in structural analysis coherently with a design approach as assumed in main international guidelines (CNR DT 215 [25] and ACI 549.4R-13 [24]). Conversely, the parametric analyses are based on linear, bilinear and trilinear behavior in order to clarify the effects of different constitutive behaviors on the cross-section analysis.

After solving the static model, normalized critical bending moment diagrams are plotted for key parameters of masonry walls like as the geometrical vertical slenderness s/H_i.

Dimensionless *P-M* interaction diagrams are plotted for several axial load levels that account for the self-weight and the interaction of other floors on the analyzed walls with the aim of evaluating the effects of retrofit systems in terms of bending capacity. It is interesting to note that for high external axial loads, the benefits of retrofit system are minor at increasing the composite mechanical ratio. This is due to the high value of neutral axis depth that causes a limited strain in the composite fiber and, consequentially, a limited contribution.

The proposed diagrams depend on normalized parameters in order to evaluate generalizable results applicable to any masonry cross section.

Comparing external load demand and capacity of cross sections, in terms of bending moment, it is possible to provide a useful fast tool to design composite retrofit systems for masonry walls in relation to an expected inundation depth depending on the composite mechanical ratio ω_c. The proposed numerical example is useful to show how to use the design charts reported in Figs. 14 and 15. In particular, the minimum composite mechanical ratio to guarantee the structural capacity can be easily evaluated given the expected inundation depth.

Future work will take into account the retrofit system effects on other local mechanisms of masonry walls, out-of-plane or in-plane, considering retrofit benefits on bending and shear capacity. In addition, earthquake damages can be taken into account for masonry walls if the epicenter is close to the coastal buildings.

Acknowledgements This research has been performed in the framework of the Italian ReLUIS project (Italian Department of the Civil Protection – years 2019-2021)

Funding Open access funding provided by Università degli Studi di Napoli Federico II within the CRUI-CARE Agreement.

Declarations

Conflicts of interest The authors declare that they have no conflict of interest.

References

1. Peiris N, Pomonis A (2005) Decembre 26, 2004 Indian ocean tsunami: vulnerability functions for loss estimation in Sri Lanka. In: *Proc., Geotechnical Engineering for Disaster Mitigation and Rehabilitation* 411–416.
2. Mallawaarachchi RS, Jayasinghe C (2008) The effects of cyclones, tsunami and earthquakes on built environments and strategies for reduced damage. J Natl Sci Found 36(1):3–14. https://doi.org/10.4038/jnsfsr.v36i1.128
3. Suppasri A, Shuto N, Imamura F et al (2013) Lessons learned from the 2011 great east Japan tsunami: performance of tsunami countermeasures, coastal buildings, and tsunami evacuation in Japan. Pure Appl Geophys 170:993–1018. https://doi.org/10.1007/s00024-012-0511-7
4. Belliazzi S, Lignola GP, Prota A (2018) Textile reinforced mortars systems: a sustainable way to retrofit structural masonry walls under tsunami loads. Int J Mason Res Innov 3(3):200–222. https://doi.org/10.1504/IJMRI.2018.093484
5. Belliazzi S, Ramaglia G, Lignola GP, Prota A (2020) Out-of-plane retrofit of masonry with FRP and FRCM systems: normalized interaction diagrams and effects on mechanisms activation. J Compos Constr (in-press). https://doi.org/10.1061/(ASCE)CC.1943-5614.0001093
6. Cavaleri L, Ciraolo G, Ferrotto MF, La Loggia G, Lo Re C, Manno G (2020) Masonry structures subjected to tsunami loads: modeling issues and application to a case study. Structures 27:2192–2207
7. Cavaleri L, Failla A, La Mendola L, Papia M (2005) Experimental and analytical response of masonry elements under eccentric vertical loads. Eng Struct 27(8):1175–1184. https://doi.org/10.1016/j.engstruct.2005.02.012
8. Ramaglia G, Lignola GP, Fabbrocino F, Prota A (2017) Impact of natural fibers on the ultimate behaviour of masonry elements. InL Proc. 23rd Congresso Associazione Italiana di Meccanica Teorica e Applicata (AIMETA 2017), Salerno, Italy, 4–7 September, 2017
9. Belliazzi S, Ramaglia G, Lignola GP, Prota A (2021) Out-of-plane retrofit of masonry with fiber-reinforced polymer and fiber-reinforced cementitious matrix systems: normalized interaction diagrams and effects on mechanisms activation. J Compos Constr 25(1):04020081. https://doi.org/10.1061/(ASCE)CC.1943-5614.0001093
10. Faella C, Martinelli E, Camorani G, Aiello MA, Micelli F, Nigro E (2011) Masonry columns confined by composite materials: design formulae. Compos Part B Eng 42:705–716. https://doi.org/10.1016/j.compositesb.2011.02.024
11. Lignola GP, Nardone F, Prota A, Manfredi G (2012) Analytical model for the effective strain in FRP-wrapped circular RC columns. Compos Part B Eng 43:3208–3218. https://doi.org/10.1016/j.compositesb.2012.04.007
12. Zinno A, Lignola GP, Prota A, Manfredi G, Cosenza E (2010) Influence of free edge stress concentration on effectiveness of FRP confinement. Compos Part B Eng 41:523–532. https://doi.org/10.1016/j.compositesb.2010.07.003
13. Ramaglia G, Fabbrocino F, Lignola GP, Prota A (2019) Unified theory for flexural strengthening of masonry with composites. Materials 12(4):680. https://doi.org/10.3390/ma12040680
14. Fabbrocino F, Ramaglia G, Lignola GP, Prota A (2019) Ductility-based incremental analysis of curved masonry structures. Eng Fail Anal 97:653–675. https://doi.org/10.1016/j.engfailanal.2019.01.027
15. Asprone D, Cadoni E, Iucolano F, Prota A (2014) Analysis of the strain-rate behavior of a basalt fiber reinforced natural hydraulic mortar. Cement Concr Compos 53:52–58. https://doi.org/10.1016/j.cemconcomp.2014.06.009
16. Cavaleri L, Fossetti M, Papia M (2009) Modeling of out-of-plane behavior of masonry walls. J Struct Eng 135(12):1522–1532. https://doi.org/10.1061/(asce)0733-9445(2009)135:12(1522)
17. Ma Z, Cooper P, Daly D, Ledo L (2012) Existing building retrofits: methodology and state-of-the-art. Energy Build 55:889–902. https://doi.org/10.1016/j.enbuild.2012.08.018
18. Lignola GP, Caggegi C, Ceroni F, De Santis S, Krajewski P, Lourenço PB et al (2017) Performance assessment of basalt FRCM for retrofit applications on masonry. Compos Part B Eng 128:1–18. https://doi.org/10.1016/j.compositesb.2017.05.003
19. Grande E, Milani G, Sacco E (2008) Modelling and analysis of FRP-strengthened masonry panels. Eng Struct 30(7):1842–1860. https://doi.org/10.1016/j.engstruct.2007.12.007
20. Giamundo V, Lignola GP, Maddaloni G, da Porto F, Prota A, Manfredi G (2016) Shaking table tests on a full-scale unreinforced and IMG retrofitted clay brick masonry barrel vault. Bull Earthq Eng 14(6):1663–1693. https://doi.org/10.1007/s10518-016-9886-7

21. D'Ambra C, Lignola GP, Prota A, Sacco E, Fabbrocino F (2018) Experimental performance of FRCM retrofit on out-of-plane behaviour of clay brick walls. Compos Part B Eng 148:198–206. https://doi.org/10.1016/j.compositesb.2018.04.062
22. Belliazzi S, Lignola GP and Prota A. (2020) Simplified approach to assess the vulnerability of masonry buildings under tsunami loads. In: Proceedings of the Institution of Civil Engineers-Structures and Buildings, 1-13, doi: https://doi.org/10.1680/jstbu.20.00147
23. Belliazzi S, Lignola GP, Di Ludovico M, Prota A (2021) Preliminary tsunami analytical fragility functions proposal for Italian coastal residential masonry buildings. Structures 31:68–79. https://doi.org/10.1016/j.istruc.2021.01.059
24. ACI 549.4R-13 (2013) Guide to design and construction of externally bonded fabric reinforced cementitious matrix (FRCM) systems for repair and strengthening concrete and masonry structures. American Concrete Institute, Farmington Hills, Michigan, U.S.A.
25. CNR Dt 215 (2018) Guide for the design and construction of externally bonded fiber reinforced cementitious matrix systems for strengthening existing structures. National Research Council, Rome, Italy
26. Lourenço PB (1998) Experimental and numerical issues in the modelling of the mechanical behaviour of masonry. Structural Analysis of Historical Constructions, 1998.
27. Eurocode 6 (2006) General rules for reinforced and unreinforced masonry structures, part 1.1. Eurocode 6. European Committee for Standardization, Brussels, Belgium
28. Kwiecień A, de Felice G, Oliveira DV, Zając B, Bellini A, De Santis S, Ghiassi B, Lignola GP, Lourenço PB, Mazzotti C, Prota A (2016) Repair of composite-to-masonry bond using flexible matrix. Mater Struct 49:2563–2580. https://doi.org/10.1617/s11527-015-0668-5
29. Bilotta A, Ceroni F, Lignola GP, Prota A (2017) Use of DIC technique for investigating the behaviour of FRCM materials for strengthening masonry elements. Compos Part B Eng 129:251–270. https://doi.org/10.1016/j.compositesb.2017.05.075
30. La Mendola L, Accardi M, Cucchiara C, Licata V (2014) Nonlinear FE analysis of out-of-plane behaviour of masonry walls with and without CFRP reinforcement. Constr Build Mater 54:190–196. https://doi.org/10.1016/j.conbuildmat.2013.12.068
31. Lignola GP, Giamundo V, Prota A, Cosenza E (2014) A unified theory for RC cross sections up to ultimate load, including hardening or softening of concrete. In: Proc. of the 4th Fib Congress 2014, Mumbai, India 10–14
32. ASCE7–16 (2017) Minimum design loads for buildings and other structures. American Society of Civil Engineering, Reston, USA
33. FEMA P-646 (2012) Guidelines for design of structures for vertical evacuation from tsunamis. Federal Emergency Management Agency, Redwood City, California
34. Fukuyama H, Kato H, Ishihara T, Tajiri S, Tani M, Okuda Y, Kabeyasawa T, Nakano Y (2011) Structural design requirement on the tsunami evacuation buildings (SDRTEB). Japanese Ministry of Land, Infrastructure, Transportation and Tourism MLIT
35. Okada T, Sugano T, Ishikawa T, Ohgi T, Takai S, Hamabe C (2005) Structural Design Method of Building for Tsunami Resistance. Building Technology Research Institute, The Building Center of Japan